Geophysical Exploration for Podiform Chromite Occurrences in the Quesnel Terrane, South-Central British Columbia (NTS 082L/04)

A.R. Branson[1], **Queen's University, Kingston, Ontario, drew.branson@queesu.ca**

C.A. Walter, Queen's University, Kingston, Ontario

G.R. Olivo, Queen's University, Kingston, Ontario

A. Braun, Queen's University, Kingston, Ontario

G. Fotopoulos, Queen's University, Kingston, Ontario

Branson, A.R., Walter, C.A., Olivo, G.R., Braun, A. and Fotopoulos, G. (2020): Geophysical exploration for podiform chromite occurrences in the Quesnel terrane, south-central British Columbia (NTS 082L/04); *in* Geoscience BC Summary of Activities 2019: Minerals, Geoscience BC, Report 2020-01, p. 13–22.

Introduction

Podiform chromite deposits represent approximately 25% of global chromite production, a production share that has been consistent for the past 50 years (Mosier et al., 2012). Chromium is an essential metal for stainless-steel production and is one of the 35 minerals identified in the United States as being "critical" (i.e., a secure and reliable supply is needed; U.S. Department of the Interior, 2018). Worldwide, production of chromium is currently dominated by, in decreasing order of importance, South Africa, Turkey, Kazakhstan and India (U.S. Geological Survey, 2019). The last known chromite production in Canada was in 1948 from the Union Carbide Company's 'Montreal' pit in the Black Lake area of Quebec (Eardley-Wilmot, 1948). Its designation as a critical mineral with no domestic supply indicates the need to investigate possible domestic sources. The primary issue facing exploration for podiform chromite is the discontinuous nature and small size of the deposits. Podiform chromite occurs in lenticular bodies in the lower portions of ophiolitic sequences, particularly in the upper (500—1000 m) part of the tectonite zone in the host harzburgite (Eckstrand et al., 1995). British Columbia has demonstrated historical potential along a chain of obducted ophiolite sequences that runs parallel to the accretionary arc along the margins of the Quesnel Terrane. The correlation between the terrane margins and known podiform chromite occurrences is shown in Figure 1. This project investigates the region surrounding one such known occurrence, located on the Bart mineral claims (#1057772; Strafehl, 2019), 25 km northwest of Kelowna.

[1]*The lead author is a 2019 Geoscience BC Scholarship recipient.*

This publication is also available, free of charge, as colour digital files in Adobe Acrobat® PDF format from the Geoscience BC website: http://www.geosciencebc.com/updates/summary-of-activities/.

Obducted ophiolites are typically highly deformed and altered by serpentinization. The process of serpentinization results in the formation of magnetite, which leads to a strong residual magnetic-field anomaly over the ophiolitic ultramafic rocks (Parvar et al., 2017). The high magnetic susceptibility of these serpentinized rocks makes magnetic surveys an effective tool for mapping the extent and structure of ophiolitic sequences. It must be noted that chromite has a low magnetic susceptibility and therefore must be detected using an indirect approach: measuring the serpentinized areas and then investigating if chromite is present through non-geophysical means, such as geochemical sampling and drilling.

Geology

The Bart mineral claims are dominated by the Permian Chapperon Group, which is generally interpreted as a fault-bounded, obducted ophiolite complex (Cui et al., 2017). The regional-scale geology and ground-magnetic survey data may be seen in Figure 2. The Chapperon Group consists of metamorphosed siliceous and calcareous argillites, greenschists of volcanic and sedimentary origin, and minor serpentinized harzburgite (also identified as dunite by Cairnes, 1932) in pelitic and volcanic rocks (Cui et al., 2017). Within the Chapperon Group are oblong bands of ultramafic intrusive rocks striking approximately 330° and known to host podiform chromite occurrences. These ultramafic units are historically known as the Old Dave intrusions. These comprise primarily dark green serpentine that often weathers to a deep orange-red but is sometimes coated with a thin, semitransparent, whitish, talcose film (Cairnes, 1932). Thin-section analysis reveals different stages of alteration, from abundant small grains of olivine occurring in a meshwork of serpentine to instances in which no traces of unaltered olivine remain (Cairnes, 1932). Other common minerals include similarly altered pyroxene, talc, chlorite, magnetite, asbestos and chromite (Cairnes, 1932).

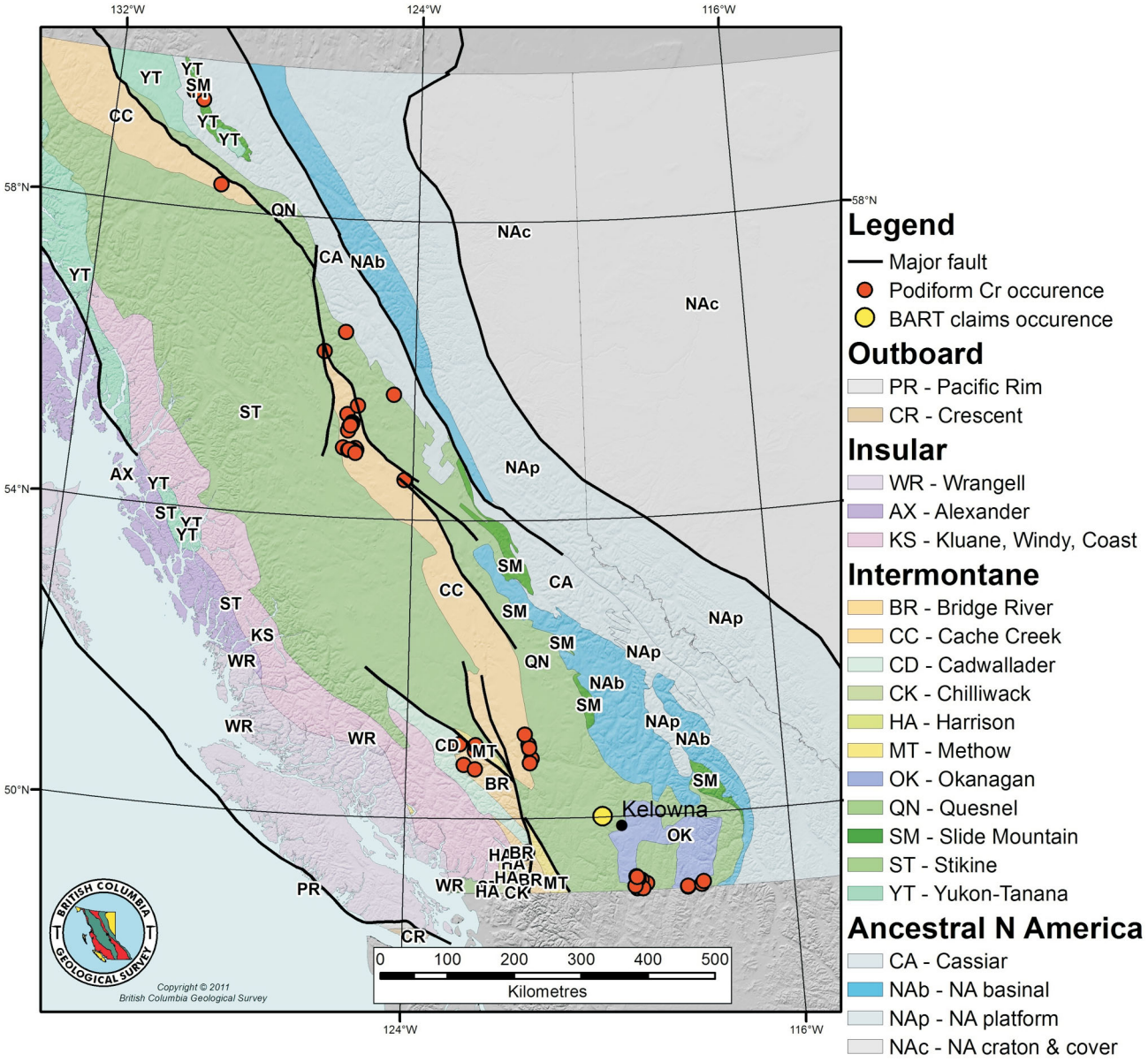

Figure 1. Terranes of British Columbia with known podiform chromite occurrences indicated. Base map from BC Geological Survey (2011), modified with MINFILE data from BC Geological Survey (2019).

The Devonian to Permian Harper Ranch Group, located east of the Chapperon Group, comprises Carboniferous to Permian arc clastic rocks (limestone, sandstone and mudstone) that form the basement to the Quesnel terrane (Beatty et al., 2006). The Chapperon and Harper Ranch groups are unconformably overlain by the Upper Triassic to Lower Jurassic Nicola Group (Cui et al., 2017). The Nicola Group comprises the following sedimentary facies of Upper Triassic age: shale, argillite, siltstone, sandstone, phyllite, tuff, local polymict conglomerate, limestone, greenstone and chloritic phyllite (Cui et al., 2017). These units were intruded into and are abutted by intermediate intrusive rocks to the southwest that comprise, in order of lessening abundance, granodiorite, quartz diorite, quartz monzonite and lesser monzonite, diorite and gabbro, emplaced during the late Triassic to early Jurassic (Cui et al., 2017). Overlying the region in the Eocene period is the Penticton Group, comprising volcanic rocks that include mixed alkalic and calcalkaline transtensional volcanic rocks and associated fluvial and lacustrine sedimentary rocks, hornblende-biotite-quartz-feldspar porphyry and biotite-hornblende-plagioclase porphyry (Cui et al., 2017). Abutted against the east side of the serpentinized belt is a parallel layer of discontinuous marble of sedimentary origin. Apart from the Penticton Group, all the geological units in the study area are components of the Quesnel terrane.

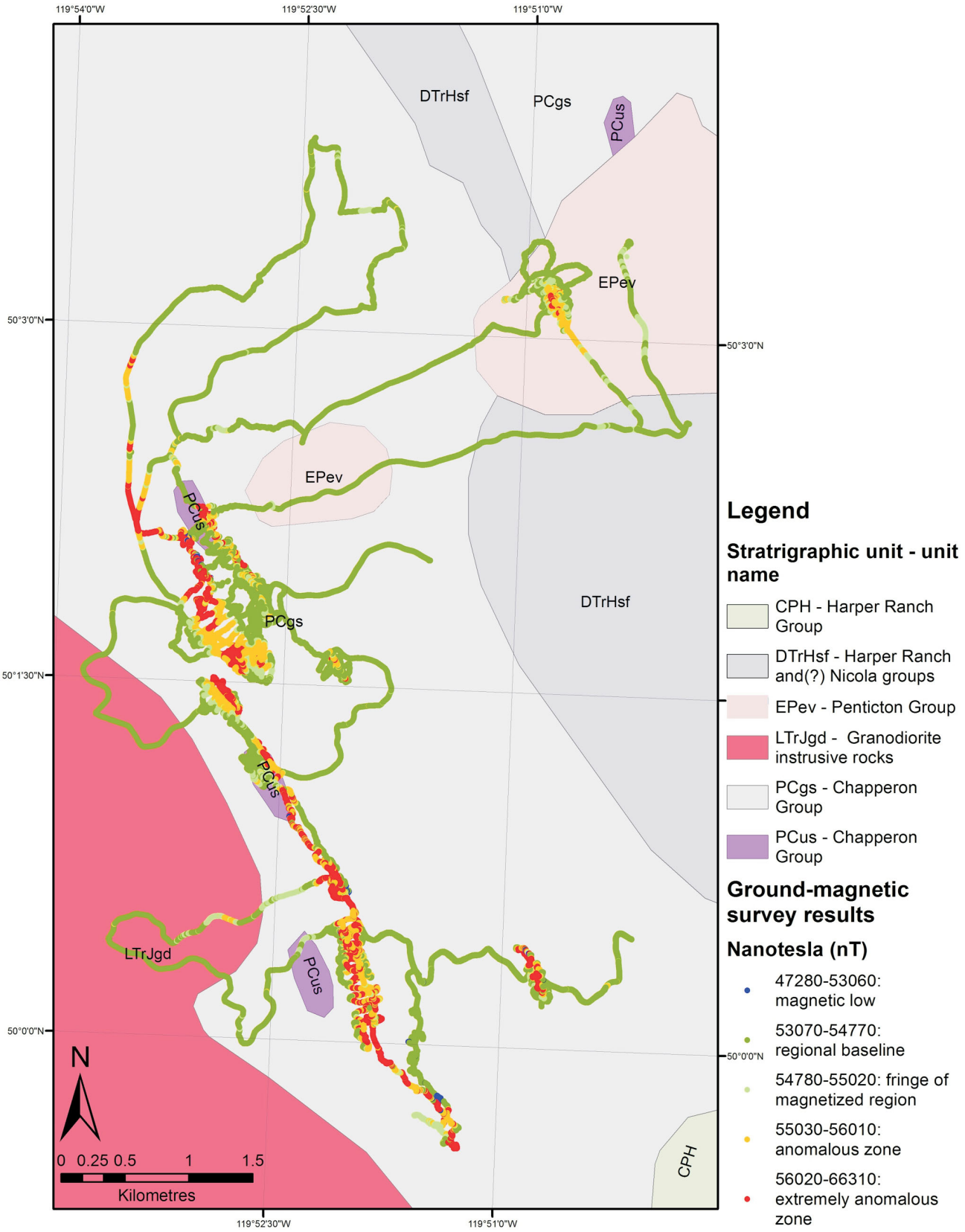

Figure 2. Regional geology of the Bart claims (#1057772; Strafehl, 2019) and ground-magnetic survey data with a manually defined discrete colour-scale, grouping distinct subsets of magnetic intensities (regional geological data from Cui et al., 2017).

Thin-section analysis was done on a sample taken from one of the known chromite pods on the property and a sample of the serpentinized ultramafic rocks that host the occurrence and are shown in Figures 3 and 4, respectively.

The clasts in Figure 3 comprise massive chromite dominated by a brittle fracture system, which was infilled by serpentine. The clasts also have inclusions of unknown opaque minerals, which exhibit a higher reflectance than

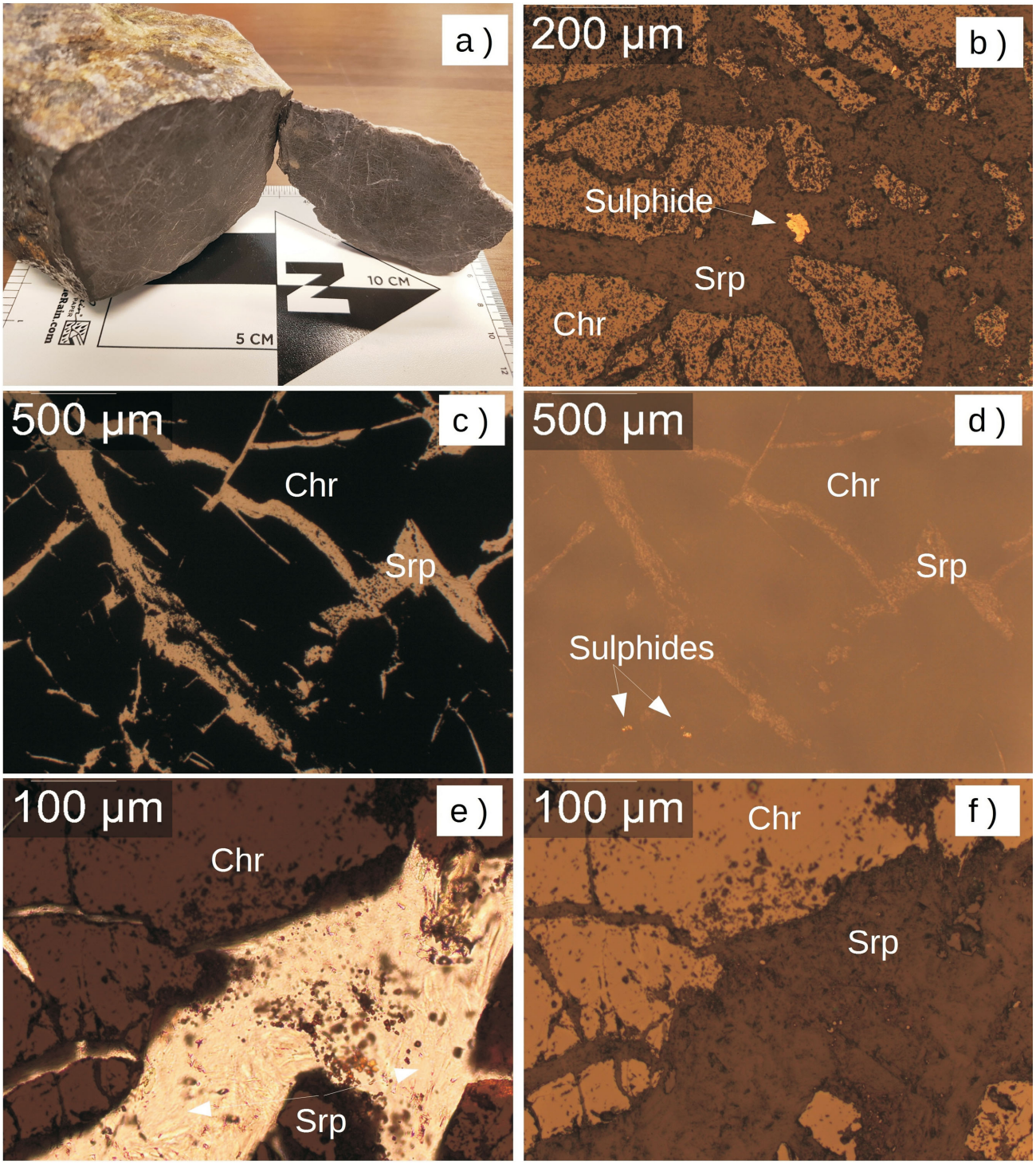

Figure 3. Sample **(a)** and photomicrographs from a known chromite pod: **b, d)** reflected-light images illustrating the fracture system that dominates the sample; chromite (Chr), which makes up 70–90% of the section, was brittlely deformed, resulting in serpentine (Srp)–filled fractures throughout the sample; unknown sulphide minerals occur throughout these fractures; **c)** transmitted-light image (with the same field of view as (d), illustrating the brittle deformation that the sample underwent; **e, f)** transmitted-light (e) and reflected light (f) views of the opaque grains hosted within the serpentine matrix.

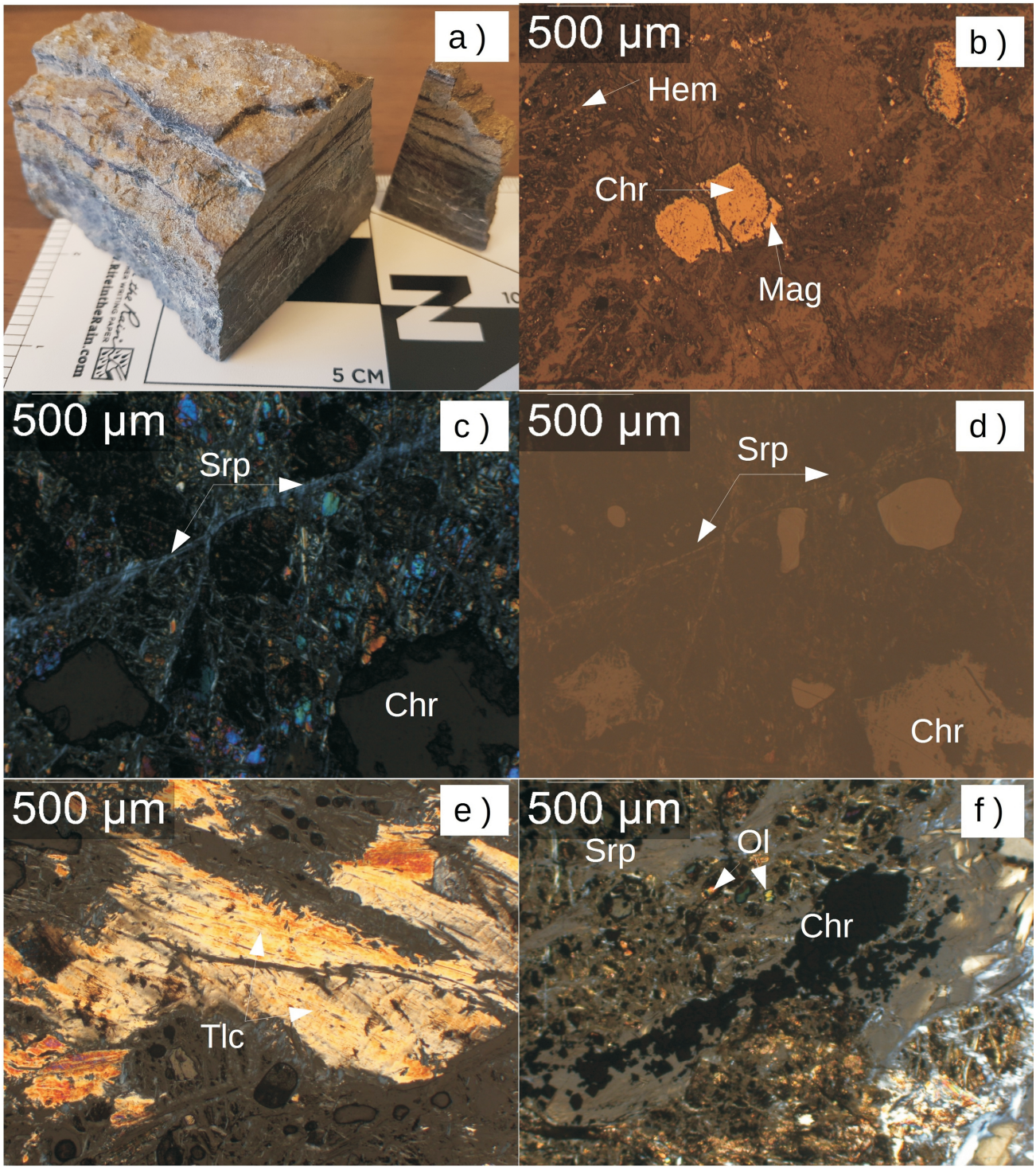

Figure 4. Typical sample **(a)** of the serpentinized ultramafic rocks that occur within the Chapperon Group and photomicrographs illustrating its mineralogy: **b)** reflected-light image of a large chromite (Chr) grain with replacement by magnetite (Mag) on the periphery of the grain, disseminated hematite (Hem) in the surrounding matrix; **c)** cross-polarized image illustrating serpentine (Srp)–filled fracture through heavily altered host; **d)** same field of view as (c) with reflected light, illustrating the moderately reflective chromite grains; **e)** cross-polarized image displaying talc (Tlc); **f)** cross-polarized image showing an accumulation of chromite grains along a heavily deformed trend in the section, hosted within remnant olivine (Ol) not destroyed by the serpentinization process.

the host chromite. The reflective inclusions may also be seen in several of the other fractures. These are likely to be sulphide minerals such as chalcopyrite or pentlandite, which will be investigated in the near future by scanning electron microscope (SEM) analysis.

The serpentinized ultramafic sample in Figure 4 was determined to consist primarily of serpentine and talc, with remnant olivine as well as opaque minerals in two modes of occurrence: disseminated throughout the section and hosted in concentrated layers as a result of metamorphic processes. These opaque minerals are believed to consist of chromite, magnetite and minor hematite. The chromite and magnetite are associated with each another, with chromite making up the core of the opaque grains and the outside altered to magnetite in many samples. This provides an explanation for the strong magnetic signal generated by these ultramafic rocks.

Ground Magnetometry Survey

The primary survey method used for delineating the extent of the serpentinized regions is ground magnetometry using a GEM Systems GSM-19T proton-precession magnetometer. Positioning was achieved using a NovAtel single-frequency GPS receiver with an advertised accuracy of 1.5 m in the horizontal plane. The GPS antenna was mounted on the GEM systems GSM-19T sensor staff, approximately 2 m above ground level. The magnetometer sampling frequency was set to 0.5 sample/second. Approximately 165 line-km were collected, assuming a 4 km/h walking speed, with 74 281 filtered observations collected in nanoteslas (nT) over the 10-day ground magnetic survey (June 18–28, 2019). A reference station for monitoring diurnal variations was not available. However, since the target anomalies were an order of magnitude larger than the diurnal signals, this was deemed to be a noncritical issue.

The primary targets for exploration were the regions of serpentinization within the ultramafic Chapperon Group, which follows a north-northwesterly structural trend. This trend dominates the joint patterns and schistosity, and controls the extent of the Chapperon and Harper Ranch groups in this region. This interpretation is based on the orientation of the purple lobes within the Chapperon Group shown in Figure 2. In order to target the north-northwest-trending serpentinized regions, large-scale (750–3000 m line spacing, depending on accessibility) perpendicular transects of this trend were made across the Chapperon Group. Anomalous zones were identified in the field and followed up with high resolution local grid surveys on subsequent days.

The magnetic data were interpolated using natural neighbour interpolation, and a discrete colour scale was applied based on geological interpretations from field observations (Figure 5). Natural-neighbour interpolation is an algorithm that, for a subset of data surrounding a query point, constructs a Voronoi diagram for the given data points and the Voronoi polygon for the query point. The proportion of overlap between the query polygon and the adjacent cells determines the weights applied for the calculation of the point value (Esri, 2016).

Interpretations

Geological interpretations were made based on a combination of magnetic signatures, field mapping and observations of geology. Based on field observations, the colour scale for magnetic intensity shown in Figures 2, 5 and 7 was selected to separate the magnetic data into geologically meaningful groups. This clustering resulted in the grouping of very high magnetic signals produced within the serpentinized zone (56 020–66 310 nT), the average signal observed within the serpentinized zone (55 030–56 010 nT) and the slightly lower signal on the fringe of this zone (54 660–55 010 nT). Based on the strong magnetic signal generated by the serpentinization of the ultramafic rocks and ground observations of the geology, the delineation of the serpentinized ultramafic rocks was reviewed as shown in Figure 6.

The geological interpretations in Figure 6 indicate several fault structures, along with strike-slip motion. These faults are oriented primarily in two parallel sets, one with sinistral strike-slip at approximately 300° and the other with dextral strike-slip at approximately 355°. Based on this pattern of strike-slip faults, it is interpreted that these faults make up a conjugate fault set, which is reacting to a north-northwest-oriented primary stress field as a result of regional-scale tectonic forces. This may be the result of a regional-scale dextral shear system that is present throughout the western cordillera (Mazzotti et al., 2008). Interpretations of the fault systems can be seen in Figure 7.

Conclusions

The data collected this field season provided the highest resolution magnetometer data to date for this area. The finer resolution of this survey has enabled more precise interpretations regarding the extent of the serpentinized zone and improved interpretations of the orientation of the fault structures. There remains some uncertainty regarding the exact orientation of these fault structures as observed during fieldwork, so these interpretations are based mainly on magnetic and topographic features. Detailing the full extent of the serpentinized ultramafic rocks will allow for more effective rock- and soil-sampling programs, which may result in the discovery of chromite pods of potential economic importance. Of additional interest, the faults in the area may have acted as fluid conduits for hydrothermal mineralization, evidence of which was observed in the area as glacially transported rock samples. Improved under-

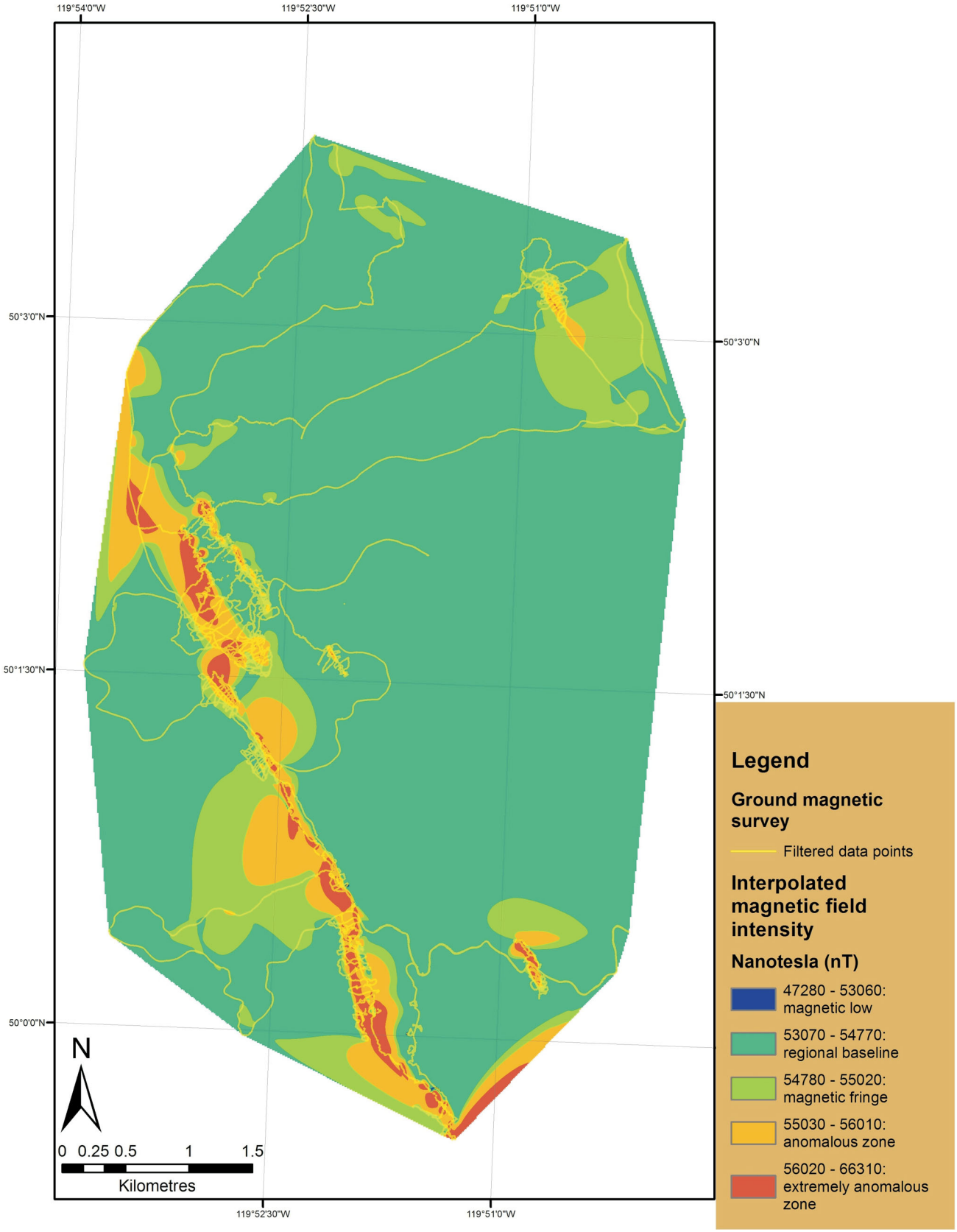

Figure 5. Natural-neighbour–interpolated magnetic-intensity data with a discrete colour scale reflecting field observations of distinct groups. Data points used in the interpolation are displayed in yellow to allow identification of interpolation and edge effects.

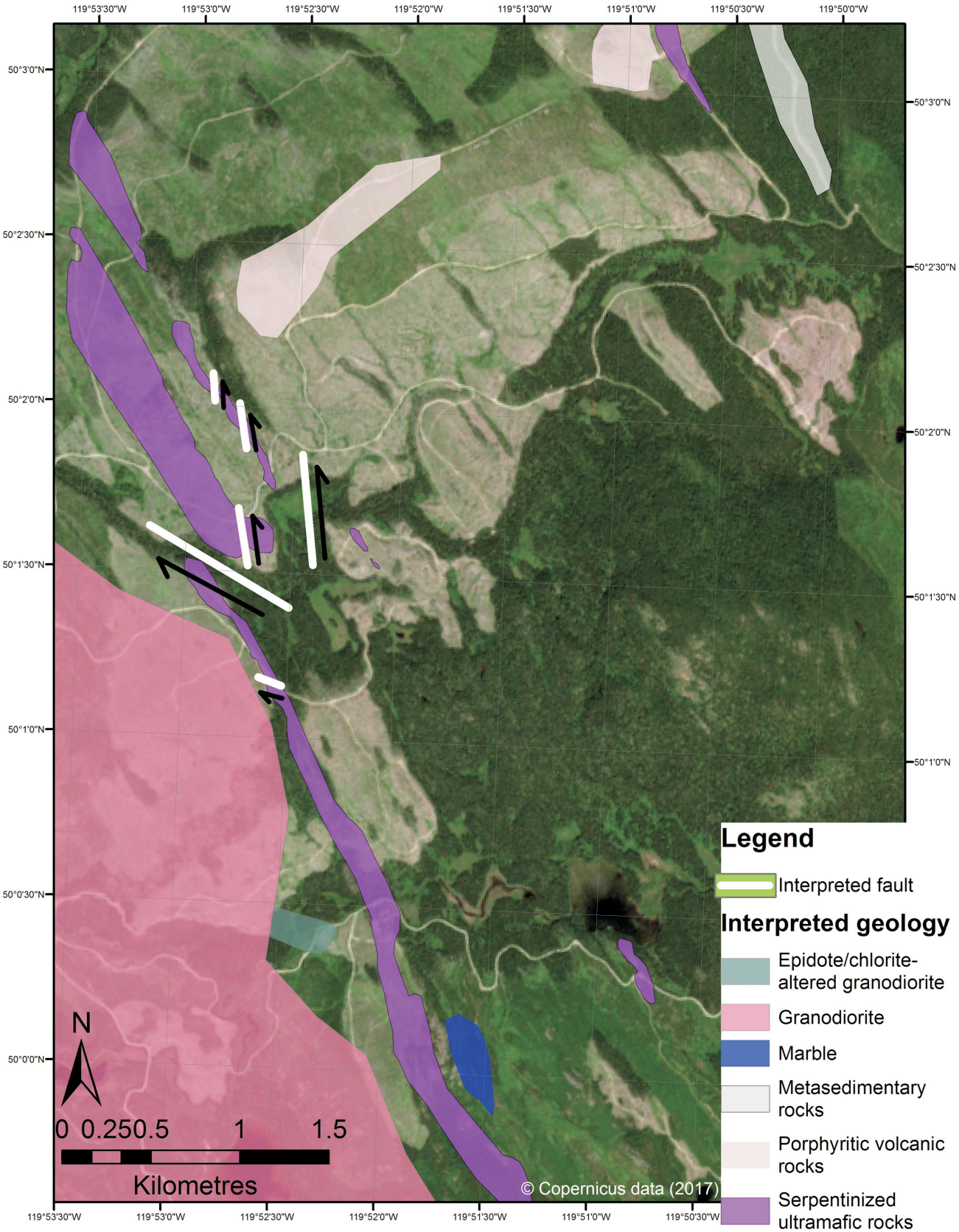

Figure 6. Geological and structural interpretations based on ground-magnetic survey and geological observations. Background imagery from Copernicus (2017).

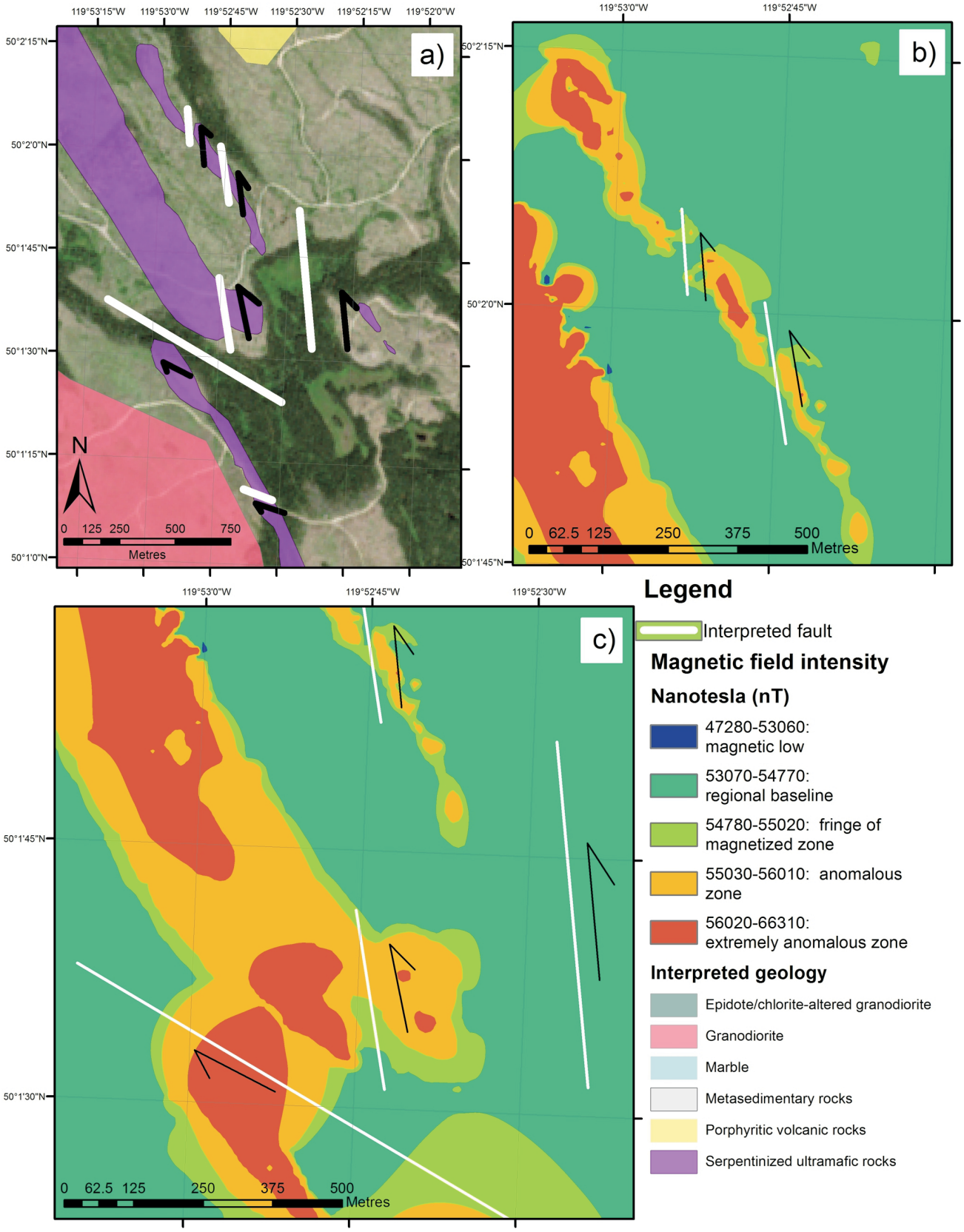

Figure 7. a) Interpreted geological and structural features in the northern part of the survey area, with supporting magnetic-field data, at 1:20 000 scale. Smaller scale subsets (1:8 000) of the data in (a), illustrating the structural interpretations with supporting interpolated and point (to illustrate data density used in interpolation) magnetic-field data for **b)** north-striking fault system in the northeastern ridge, and **c)** evidence of conjugate faults through the southern northwest-trending gully and the central lobe, which was displaced northward.

standing of these fault structures may generate targets for exploration of hydrothermal mineral occurrences.

Future Work

In order to better resolve the distribution of magnetic susceptibility within the serpentinized ultramafic belt, an unmanned aerial vehicle (UAV)–borne aeromagnetic survey is planned for the spring of 2020. This will allow total-magnetic-field data to be collected at a high resolution over the tops of densely forested areas and steep gullies where collecting terrestrial total-magnetic-field measurements was not physically possible. This UAV magnetometry is also capable of achieving higher spatial resolution than a manned airborne survey. This UAV-borne total-magnetic-field data will enable gaps in the terrestrial magnetic data to be filled, observation of additional fault structures and the ability to better resolve areas within the serpentinized ultramafic rocks that may host chromite. An SEM analysis will be conducted to verify mineral interpretations from the thin sections and to determine the composition of the observed sulphide inclusions.

Acknowledgments

The authors thank M. MacDougall for reviewing this paper and Geoscience BC, Redline Minerals Inc. and Mitacs for their support of this project. They also acknowledge the Society of Economic Geologists Foundation (SEGF) for a student research grant from the Hugo Dummet Discovery Fund to C.A. Walter for fieldwork.

References

BC Geological Survey (2011): BC terranes 2011; BC Ministry of Energy, Mines and Petroleum Resources, BC Geological Survey, map, 1:8 000 000 scale, URL <https://www2.gov.bc.ca/assets/gov/farming-natural-resources-and-industry/mineral-exploration-mining/bc-geological-survey/mineral-inventory/bc_terranes_2011.pdf> [November 2019].

BC Geological Survey (2019): MINFILE BC mineral deposits database; BC Ministry of Energy, Mines and Petroleum Resources, BC Geological Survey, URL <http://minfile.ca/> [November 2019].

Beatty, T.W., Orchard, M.J. and Mustard, P.S. (2006): Geology and tectonic history of the Quesnel terrane in the area of Kamloops, British Columbia; *in* Paleozoic Evolution and Metallogeny of Pericratonic Terranes at the Ancient Pacific Margin of North America, Canadian and Alaskan Cordillera, M. Colpron and J. Nelson (ed.), Geological Association of Canada, Geological Association of Canada, Special Paper 45, p. 483–504.

Cairnes, C.E. (1932): Mineral resources of northern Okanagan Valley, BC; *in* Geological Survey, Summary Report, 1931, Part A, Canada Department of Mines, Ottawa, Ontario, p. 66A–109A, URL <http://ftp.geogratis.gc.ca/pub/nrcan_rncan/publications/ess_sst/293/293756/sum_rep_1931_a.pdf> [November 2019].

Copernicus (2017): Sentinel-2A satellite true colour image: image granule s2a_msil1c_20170702t185921_n0205_r013_t10uga_20170702t190708; Copernicus, European Space Agency, Open Access Hub, URL <https://scihub.copernicus.eu/dhus/#/home> [November 2019].

Cui, Y., Miller, D., Schiarizza, P. and Diakow, L. J. (2017): British Columbia digital geology. BC Ministry of Energy, Mines and Petroleum Resources, BC Geological Survey, Open File 2017-8, 9 p. (data version 2018-04-05), URL <https://www2.gov.bc.ca/gov/content/industry/mineral-exploration-mining/british-columbia-geological-survey/geology/bcdigitalgeology> [November 2019].

Eardley-Wilmot, V.L. (1948): Chromium; *in* The Canadian Mineral Industry in 1948, Canada Department of Mines and Technical Surveys, no. 829, p. 9–11.

Eckstrand, O.R., Sinclair, W.D. and Thorpe, R.I., editors (1995): Geology of Canadian Mineral Deposit Types; Geological Survey of Canada, Geology of Canada, no. 8, 640 p. (also Geological Society of America, The Geology of North America, v. P-1), URL <https://doi.org/10.4095/207944> [November 2019].

Esri (2016): How Natural Neighbor works; Environmental Systems Research Institute, URL <http://desktop.arc gis.com/en/arcmap/10.3/tools/spatial-analyst-toolbox/how-natural-neighbor-works.htm> [November 2019].

Mazzotti, S., Leonard, L.J., Hyndman, R.D. and Cassidy, J.F. (2008): Tectonics, dynamics, and seismic hazard in the Canada-Alaska cordillera; *in* Active Tectonics and Seismic Potential of Alaska, J. Freymueller, P.J. Haeussler, R. Wesson and G. Ekstrom (ed.), American Geophysical Union (AGU), Geophysical Monograph Series, Volume 179, p. 297–319, URL <https://doi.org/10.1029/179GM17> [November 2019].

Mosier, D., Singer, D., Moring, B. and Galloway, J. (2012): Podiform chromite deposits—database and grade and tonnage models; U.S. Geological Survey Scientific Investigations Report 2012-5157, 45 p., URL <https://pubs.usgs.gov/sir/2012/5157/sir2012-5157_text.pdf?fbclid=IwAR0YxIvRJNfRUJ8iyFVPs-iGgpSMgvvP781XNFTQmU0lTIw-SD_O29hSBxw> [November 2019].

Parvar, K., Braun, A., Layton-Matthews, D. and Burns, M. (2017): UAV magnetometry for chromite exploration in the Samail ophiolite sequence, Oman; Journal of Unmanned Vehicle Systems, v. 6, no. 1, p. 57–69, URL <https://doi.org/10.1139/juvs-2017-0015> [November 2019].

Strafehl, R. (2019): Geologic and geochemical assessment report on the Bart claims (NTS 082L/04W); BC Ministry of Energy, Mines and Petroleum Resources, BC Geological Survey, Assessment Report Indexing System (ARIS), Assessment Report 38145, 89 p., URL <https://aris.empr.gov.bc.ca/search.asp?mode=repsum&rep_no=38145> [November 2019].

U.S. Department of the Interior (2018): Final list of critical minerals 2018; Federal Register, v. 83, no. 97, May 18, 2018, p. 23295–23296, URL <https://www.govinfo.gov/content/pkg/FR-2018-05-18/pdf/2018-10667.pdf> [November 2019].

U.S. Geological Survey (2019): Mineral commodity summaries 2019: chromium; U.S. Geological Survey, Washington, DC, p. 46–47, URL <https://doi.org/10.3133/70202434> [November 2019].